DEVELOPMENTAL DYNAMICS 247:1146–1159, 2018
DOI: 10.1002/dvdy.24668

Cre/*lox*-controlled Spatiotemporal Perturbation of FGF Signaling in Zebrafish

Lucia Kirchgeorg,[1] Anastasia Felker,[1] Marek van Oostrom, Elena Chiavacci, and Christian Mosimann*

Institute of Molecular Life Sciences, University of Zürich, Zürich, Switzerland

Background: Spatiotemporal perturbation of signaling pathways in vivo remains challenging and requires precise transgenic control of signaling effectors. Fibroblast growth factor (FGF) signaling guides multiple developmental processes, including body axis formation and cell fate patterning. In zebrafish, mutants and chemical perturbations affecting FGF signaling have uncovered key developmental processes; however, these approaches cause embryo-wide perturbations, rendering assessment of cell-autonomous vs. non-autonomous requirements for FGF signaling in individual processes difficult.
Results: Here, we created the novel transgenic line *fgfr1-dn-cargo*, encoding dominant-negative Fgfr1a with fluorescent tag under combined Cre/*lox* and heatshock control to perturb FGF signaling spatiotemporally. Validating efficient perturbation of FGF signaling by *fgfr1-dn-cargo* primed with ubiquitous CreERT2, we established that primed, heatshock-induced *fgfr1-dn-cargo* behaves similarly to pulsed treatment with the FGFR inhibitor SU5402. Priming *fgfr1-dn-cargo* with CreERT2 in the lateral plate mesoderm triggered selective cardiac and pectoral fin phenotypes without drastic impact on overall embryo patterning. Harnessing lateral plate mesoderm-specific FGF inhibition, we recapitulated the cell-autonomous and temporal requirement for FGF signaling in pectoral fin outgrowth, as previously inferred from pan-embryonic FGF inhibition.
Conclusions: As a paradigm for rapid Cre/*lox*-mediated signaling perturbations, our results establish *fgfr1-dn-cargo* as a genetic tool to define the spatiotemporal requirements for FGF signaling in zebrafish. *Developmental Dynamics 247:1146–1159, 2018*. © 2018 Wiley Periodicals, Inc.

Key words: Zebrafish; signaling; Cre/*lox*; transgenes; heatshock; FGF

Submitted 13 June 2018; First Decision 13 August 2018; Accepted 30 August 2018; Published online 12 October 2018

Introduction

The zebrafish has become a key model to study vertebrate development using the increasing number of available mutants and transgenic strains. While generation of loss-of-function mutants is now accessible with the latest advances in genome editing, the modulation of gene activity and of signaling pathways in space and time during development remains a key challenge in the field. Complementing chemical genetics approaches, transgenic constructs that ubiquitously and constitutively express candidate genes or signaling modulators are frequently applied for over- or misexpression studies. The challenge with such constitutive transgenes remains the possibly detrimental impact on overall development, often precluding the generation of stable transgenic zebrafish strains due to lethality.

Transgenics based on the promoter element of the *heatshock protein 70l* (*hsp70l*) gene have been widely applied to overcome this hurdle by adding temporal control: *hsp70l* activity reacts to moderate heatshock (i.e., 37 °C), which can be harnessed to trigger transgene expression at any desired time point. This approach has been successfully established to investigate the contribution of various signaling pathways, including Wnt, FGF, and BMP, to developmental or regenerative processes in the zebrafish (Lee et al., 2005; Lewis et al., 2004; Ueno et al., 2007; Zuniga et al., 2011). Nonetheless, the activity of *hsp70l*-based transgenes is position-dependent, potentially causing leaky expression in the germ line or during the life cycle of the zebrafish that can result in undesirable or even lethal expression of the transgenic cargo. In contrast, bimodal systems such as the Gal4/*UAS* system enable more precise spatial control of transgene expression. Gal4/*UAS* works by coupling the expression of a *UAS*-controlled transgene to the activity of the *UAS*-binding Gal4 transcription factor as an effector under tissue-specific or additional drug-inducible activity (Brand and Perrimon, 1993), providing an elegant means to target candidate gene expression to any cell type with suitable Gal4 drivers (Halpern et al., 2008; Kawakami et al., 2016). The key drawback of these

Grant sponsor: Swiss National Science Foundation; Grant number: 150838.
[1]These authors contributed equally to this work.
*Correspondence to: Christian Mosimann, Institute of Molecular Life Sciences, University of Zürich, Winterthurerstrasse 190, 8057 Zürich, Switzerland. E-mail: christian.mosimann@imls.uzh.ch

Article is online at: http://onlinelibrary.wiley.com/doi/10.1002/dvdy.24668/abstract

bimodal systems remains the coupling of transgene cargo activity to effector expression, resulting in shutdown of transgene expression upon casing activity of the effector.

The Cre/*lox* system provides true uncoupling of transgene expression for precise spatiotemporal control: a Cre recombinase-expressing transgene triggers excision of a *lox*-flanked (floxed) stop cassette driven by a ubiquitous or tissue-specific regulatory element, resulting in productive expression of a signaling modulator that is then uncoupled from Cre activity (Branda and Dymecki, 2004; Rossant and Nagy, 1995). While *loxP*-flanked exons enable the generation of conditional loss-of-function alleles, the generation of such engineered alleles has remained challenging in zebrafish. Besides the invaluable use for genetic lineage tracing using reporter genes, a limited number of such floxed switch transgenes have been applied to drive transcription factors, chromatin modulators, and signaling effectors (Carney and Mosimann, 2018). Nonetheless, the generation of floxed transgenes in zebrafish has been demanding, as the recombination efficiency seems to be heavily influenced by genomic location of the transgene integration, requiring extensive screening for responsive floxed switch lines (Carney and Mosimann, 2018).

In addition to achieving tight transgene control without any potentially detrimental leaky expression, the kinetics of transgene-based signaling modulators need to be fast enough to reach functional levels in the embryo to elicit an inhibitory response: while transgenic drivers based on ubiquitously active promoter elements such as *beta-actin, ef1-α*, or *ubiquitinB* enable broad transgene expression, transgene expression upon Cre-mediated activation requires hours or even days to reach detectable levels (Carney and Mosimann, 2018; Chen et al., 2017; Hans et al., 2009; Mosimann et al., 2011). In contrast, heatshock-triggered transgenes have more rapid kinetics, and transgenic cargo under *hsp70l* promoter control is detectable less than 1 hr after heatshock (Hans et al., 2011; Hesselson et al., 2009). The so-called HOTcre approach combines the benefits of spatiotemporal transgene priming and subsequent temporal control of transgene cargo activity using *hsp70l*-controlled, floxed transgenes (Hesselson et al., 2009).

Fibroblast growth factors (FGFs) control fundamental steps during vertebrate development. FGF ligands interact with cell surface–located FGF receptor tyrosine kinases (RTKs) on signal-receiving cells (Bökel and Brand, 2013; Huang and Stern, 2005; Itoh and Konishi, 2007; Ornitz and Itoh, 2001; Plotnikov et al., 2000). FGF ligand binding induces receptor dimerization, followed by tyrosine kinase activation by transphosphorylation, and, primarily, activation of the Ras/MAPK, PLC/Ca^{2+} and PI3K/Akt cascades (Böttcher and Niehrs, 2005). The vast number of individual ligands and receptors with complex spatiotemporal expression patterns and the various downstream effects of FGF signaling have greatly complicated the study of this key signaling pathway in vertebrate development. The protein tyrosine kinase inhibitor compound SU5402 prevents transphosphorylation by competing with ATP at the FGF Receptor (FGFR) catalytic domain, allowing experimental inhibition of FGF signaling (Mohammadi et al., 1997). Embryo-wide FGF perturbation during gastrulation results in aborted development of mesodermal and posterior structures, while pathway overactivation causes embryo dorsalization (Deng et al., 1994; Kroll and Amaya, 1996; Oki et al., 2010; Ota et al., 2009; Sun et al., 1999). Additionally, functional redundancy of FGFs and FGFRs complicates the evaluation of the impact of this signaling pathway on the developmental processes (Ornitz and Itoh, 2015). In zebrafish, the mutant *acerebellar (ace/fgf8a)* features perturbed heart formation, as revealed by reduced cardiac marker expression and aberrant chamber development (Marques et al., 2008; Reifers et al., 2000). *ace* mutants also display axis formation defects and lack the midbrain-hindbrain boundary and the cerebellum (Brand et al., 1996; Reifers et al., 1998). Correspondingly, FGF signaling inhibition by SU5402 treatment does not only affect early cardiac gene expression, establishment of the myocardial progenitor pool, and organ territories within the anterior lateral plate mesoderm (LPM), it also leads to shortening of posterior axis structures and defects in brain patterning (Felker et al., 2018; Marques et al., 2008; de Pater et al., 2009; Reifers et al., 2000; Simoes et al., 2011).

Previous work has established genetically controlled signaling inhibitors based on transgenes to modulate FGF signaling. Mutant FGFR with a nonfunctional cytoplasmic kinase domain can act as a dominant-negative signaling inhibitor by forming unproductive heterodimers with native FGFR molecules, leading to their sequestration (Amaya et al., 1991; Ledda and Paratcha, 2007; Ota et al., 2009; Ullrich and Schlessinger, 1990). In zebrafish, dominant-negative Fgfr1a efficiently inhibits FGF signaling when ubiquitously driven by a heatshock-controlled *hsp70l:dn-fgfr1* transgene (Lee et al., 2005), which has been widely applied to study the influence of FGF signaling in development and regeneration (Lee et al., 2005; Lepilina et al., 2006; Neugebauer et al., 2009; Richardson et al., 2016; Shin et al., 2007). While FGF signaling significantly contributes to cardiac and limb development, more precise spatiotemporally controlled perturbation of FGF signaling by genetic means would provide a crucial approach to dissect the cell-autonomous functions and windows of action for FGF signaling.

Here, we sought to achieve rapid and cell type–specific signaling perturbations based on the Cre/*lox* system. We generated and functionally evaluated a novel transgenic zebrafish line carrying a fluorescently marked, Cre/*lox*- and heatshock-controlled transgene based on the dominant-negative form of FGF receptor 1a (Fgfr1a) to spatiotemporally perturb FGF signaling. The resulting transgene *Tg(-1.5hsp70l:loxP-STOP-loxP-fgfr1a-dn-2A-Cerulean-CAAX)*, abbreviated as *fgfr1-dn-cargo*, enables cell type–specific priming by CreERT2 recombinase and subsequent heatshock-controlled expression of Fgfr1a dominant-negative protein with concomitant blue membrane labeling. We establish that *fgfr1-dn-cargo* triggered under its controlling stimuli results in pulsed inhibition of FGF target gene control similar to pulsed SU5402-mediated chemical inhibition of the pathway. When applied to perturb FGF signaling in the LPM, *fgfr1-dn-cargo* triggered in the descendants of *drl*-expressing LPM cells resulted in selective heart and pectoral fin defects without other pan-embryonic FGF loss-of-function phenotypes. Combining this spatiotemporal inhibition, we established two windows of LPM-autonomous FGF sensitivity for pectoral fin formation. Taken together, *fgfr1-dn-cargo* provides a versatile transgenic for spatiotemporal inhibition of FGF signaling activity applicable to broad developmental and regenerative contexts in zebrafish. Further, our work outlines the application and caveats of Cre/*lox*-controlled signaling modulators.

Results

A Floxed and Heatshock-dependent Transgene to Drive Dominant-negative Fgfr1a in Zebrafish

Heterodimerization of FGFR with constitutive-active or dominant-negative forms of FGFR can sequester the native

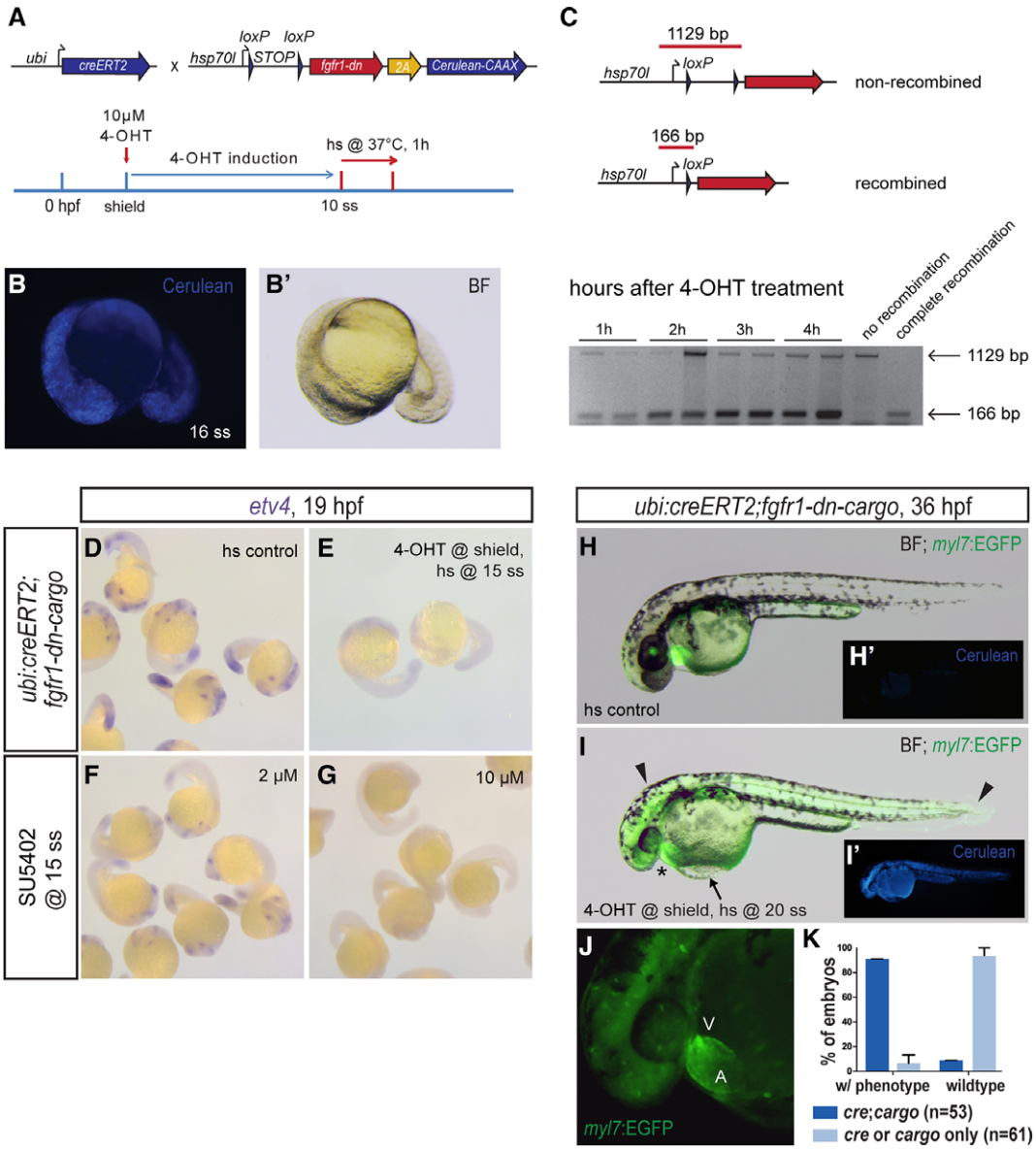

Fig. 1. Global FGF signaling perturbation using the *fgfr1-dn-cargo* transgenic line. **A**: Schematic showing the crosses and a representative treatment scheme for ubiquitous genetic FGF signaling perturbation with the *fgfr1-dn-cargo* transgenic line. Note that *fgfr1-dn-cargo* contains a *2A*-linked *Cerulean-CAAX* ORF. **B,B'**: Ubiquitous *fgfr1-dn-cargo* activation in 4-OHT– and heatshock-treated *ubi:creERT2;fgfr1-dn-cargo* transgenic embryos as shown in schematic (A) leads to ubiquitous but mosaic Cerulean-CAAX (Cerulean) expression. **C**: CreERT2-mediated ubiquitous excision of the *loxP*-flanked *STOP* cassette in *ubi:creERT2;fgfr1-dn*-cargo transgenics 4-OHT induced during early somitogenesis as detected by PCR (166 bp after recombination, 1129 bp when unrecombined). Excision of the *STOP* cassette occurs within 1 hr and gradually increases up to 4 hr after 4-OHT treatment. Shown are PCR on recombined and unrecombined transgene insertions. **D–G**: Heatshock (hs) controls, *ubi:creERT2;fgfr1-dn*-cargo embryos induced with 4-OHT at shield stage and heatshocked at 15 ss, and wild-type embryos treated with 2 or 10 µM SU5402 at 15 ss were fixed at 19 hpf and stained for *etv4* expression via mRNA in situ hybridization. Ubiquitous *fgfr1-dn-cargo* activation and concentration-dependent SU5402 treatment abolish *etv4* expression as a readout for FGF signaling activity. **H,I**: Overlay of EGFP expression on a brightfield (BF) image of a 36-hpf heatshock control and *ubi:creERT2;fgfr1-dn*-cargo embryo induced with 4-OHT at shield stage and heatshock-treated at 20 ss. Embryos with ubiquitous expression of Fgfr1-dn during late somitogenesis have a mis-looped heart (asterisk) as well as head defects and malformations in posterior tail structures (arrowheads). The heart malformations also manifest in blood pooling in front of the inflow tract of the heart, leading to a visible edema on top of the yolk (arrow). **H',I'**: Cerulean-CAAX expression in control and signaling-perturbed embryos. **J**: 7x magnification of the heart of a 4-OHT–induced and heatshock-treated *ubi:creERT2;fgfr1-dn-cargo* double transgenic (**I**) showing heart defects with a large atrium (A) and diminished ventricle (V); green background fluorescence is caused by bleedthrough of Cerulean fluorescence (see also I'). **K**: Quantification of phenotypes resulting from global FGF signaling perturbation in genetically perturbed double-transgenic *ubi:creERT;fgfr-dn*-cargo embryos and single-transgenic heatshock controls treated as indicated (I).

receptors and consequently modulate signaling activity, as achieved in ubiquitously active transgenes (Lee et al., 2005). To achieve spatiotemporal control over FGF signaling inhibition, we incorporated a dominant-negative Fgfr1a (Fgfr1a-dn) version carrying an inactivating mutation in its kinase domain (Lee et al., 2005; Ota et al., 2010) and a fluorescent marker coupled in a Cre/*lox*- and heatshock-controllable *Tol2* transgene, similar to the HOTcre approach (Hesselson et al., 2009). The resulting transgene *Tg(-1.5hsp70l:loxP-STOP-loxP-fgfr1a-dn-2A-Cerulean-CAAX,α-crystallin:YFP)* (Fig. 1A) primes *fgfr1a-dn*

expression upon Cre-mediated *loxP* recombination in the cell type and at the time of choice; subsequent heatshock treatment activates the transgene at the desired perturbation stage, and membrane-bound blue-fluorescent Cerulean-CAAX marks all cells with successfully activated transgene. Due to the strong position sensitivity of *lox* cassette transgenes (Felker and Mosimann, 2016; Mosimann et al., 2011; Mosimann and Zon, 2011), we screened more than a dozen transgenic insertions before establishing one stable transgenic line *Tg(-1.5hsp70l:loxP-STOP-loxP-fgfr1a-dn-2A-Cerulean-CAAX^{VII})*, which we call *fgfr1-dn-cargo*, that showed reproducible recombination and transgene expression efficiency.

To test the general functionality of the stable *fgfr1-dn-cargo* line, we first ubiquitously primed *fgfr1-dn* expression through recombination using the *ubi:creERT2* driver (Mosimann et al., 2011). Treating embryos with 4-OHT at shield stage and inducing transcriptional activation of the *fgfr1-dn-cargo* cassette with heatshock treatment at 10 somite stage (ss) resulted in mosaic Cerulean-CAAX expression throughout the body of double-transgenic embryos, indicating successful transgene expression (Fig. 1A,B). To analyze the precise dynamics of 4-OHT–mediated recombination of the *fgfr1-dn-cargo* transgene, we analyzed excision of the *loxP*-flanked *STOP* cassette from genomic DNA via PCR. Following ubiquitous CreERT2 recombinase activity, we robustly detected successful recombination as soon as 1 hr after 4-OHT treatment and more efficient recombination 2 hr after 4-OHT treatment, indicating fast in vivo *loxP* recombination in line with previous reports (Hans et al., 2009) (Fig. 1C).

We next tested the efficacy of FGF signaling perturbation by comparing expression of the direct FGF downstream target *etv4/pea3* (Raible and Brand, 2001; Roehl and Nüsslein-Volhard, 2001) upon global *fgfr1-dn-cargo* transgene activation or chemical inhibition of endogenous FGFRs with the established compound SU5402 (Mohammadi et al., 1997). In Cerulean-CAAX–expressing *ubi:creERT2;fgfr1-dn-cargo* double transgenics that we had primed with 4-OHT at shield stage (6 hr post-fertilization [hpf]) and heatshock-treated at 15 ss (16.5 hpf), we observed by mRNA in situ hybridization a consistent and complete loss of *etv4* expression at 20–25 ss (19 hpf) (Fig. 1D,E); we saw an equivalent effect on *etv4* expression in wild-type embryos of the same stage when treated at 15 ss with high concentrations of SU5402 (Fig. 1F,G). Activating ubiquitous Fgfr1-dn expression at 20 ss by heatshock treatment, we further detected morphological defects corresponding to phenotypes previously described global FGF signaling perturbations during late somitogenesis (Marques et al., 2008): a mis-looped heart with large atria and a diminished ventricle, lack of blood flow, plus head and posterior tail malformations (Fig. 1H–K; n = 53), all phenotypes with high penetrance (Fig. 1K). Taken together, these results indicate that our *fgfr1-dn-cargo* line provides a functional zebrafish transgene for perturbing the FGF signaling pathway by driving dominant-negative Fgfr1a.

loxP recombination efficiency in response to Cre recombinase is critical to floxed transgene functionality. To gain insight into the ubiquitous recombination efficiency of *fgfr1-dn-cargo*, we imaged *ubi:creERT2;fgfr1-dn-cargo* transgenic embryos after inducing with 4-OHT at shield stage and heatshock at 72 hpf (Fig. 2A–D). Recombined cells are easily detectable by the membrane labeling with Cerulean-CAAX, which confines to membrane compartments and the plasma membrane of *fgfr1-dn-cargo*–expressing cells (Fig. 2B). While *fgfr1-dn-cargo* potently expresses in large clones upon ubiquitously active CreERT2 exposure in diverse structures, recombination is not complete as illustrated by Cerulean-CAAX–negative clones (Fig. 2A–D; n = 13). To quantify recombination efficiency, we crossed *fgfr1-dn-cargo* to *drl:creERT2*, in which the *drl* regulatory elements drive CreERT2 in the forming LPM from late gastrulation to early somitogenesis before confining expression to cardiovascular lineages (Henninger et al., 2017; Hess et al., 2018; Mosimann et al., 2015). After 4-OHT induction at shield stage, we quantified the lineage labeling of intersomitic vessels (ISVs) at 72 hpf, which provides a dose-dependent proxy for recombination efficiency (Felker et al., 2016). We found that *drl:creERT2;fgfr1-dn-cargo* embryos had on average 62% (mean, s.d. 18.9%; median 61.5%, n = 13) labeled vessels between segments (Fig. 2E,F). Compared to *ubi:loxP-GFP-loxP-mCherry* (*ubi:Switch*), which reaches up to 100% efficiency in this assay (Felker et al., 2016; Mosimann et al., 2011), *fgfr1-dn-cargo* recombines less efficiently and causes mosaic inhibition of FGF signaling, which has to be taken into consideration when interpreting resulting phenotypes.

Dynamics of FGF Signaling Perturbation From *fgfr1-dn-cargo* Resembles Pulsed SU5402 Treatment

Heatshock-mediated transgene induction generates a pulse of *hsp70l* promoter-driven transcription, resulting in transient expression of the controlled transgene. We therefore hypothesized that our *fgfr1-dn-cargo* transgene provides pulsed inhibition of FGF signaling. To analyze the temporal dynamics of transgene expression, we compared the impact on *etv4* expression in 4-OHT– and heatshock-treated *ubi:creERT;fgfr1-dn-cargo* double transgenics; embryos exposed to SU5402 for a 4-hr pulse before washing out the drug; and Cerulean-negative single-transgenic controls (Fig. 3A). We chose 10–11 ss (14–15 hpf) to initiate FGF inhibition, as *etv4* expression is then easily detectable by mRNA in situ hybridization in several regions of the developing embryo (Fig. 3B–F).

Both in *ubi:creERT2;fgfr1-dn-cargo* double transgenics and in SU5402-treated embryos, strong reduction of *etv4* expression became detectable within 2 hr after treatment, with nearly complete absence within 4 hr after treatment (Fig. 3B,C). *etv4* expression remained broadly absent up to 6 hr after heatshock treatment or SU5402 addition (2 hr after washout) (Fig. 3D). Eight and 9 hr following transgene activation or SU5402 treatment (corresponding to 4 and 5 hr after washout), respectively, *etv4* expression was still notably reduced, but expression started to recover in both conditions, with possibly slightly slower recovery in *ubi:creERT2;fgfr1-dn-cargo* embryos (Fig. 3E,F). The dynamics of *etv4* expression in *ubi:creERT2;fgfr1-dn-cargo* double transgenics and SU5402 pulse-treated embryos reveal that ubiquitous *fgfr1-dn-cargo* transgene activation resembles chemical FGFR inhibition in respect to strength and onset dynamics. Further, the up-regulation of *etv4* expression within 8 hr after transgene activation is consistent with the notion that FGF signaling perturbation in the *fgfr1-dn-cargo* line does not occur indefinitely but as a pulse.

We further sought to analyze FGF signaling activity in embryos that were genetically or chemically perturbed during gastrulation and initiated *fgfr1-dn-cargo* expression or SU5402 treatment at shield stage (Fig. 3G). Under these conditions, we did not detect any embryos with complete absence of FGF

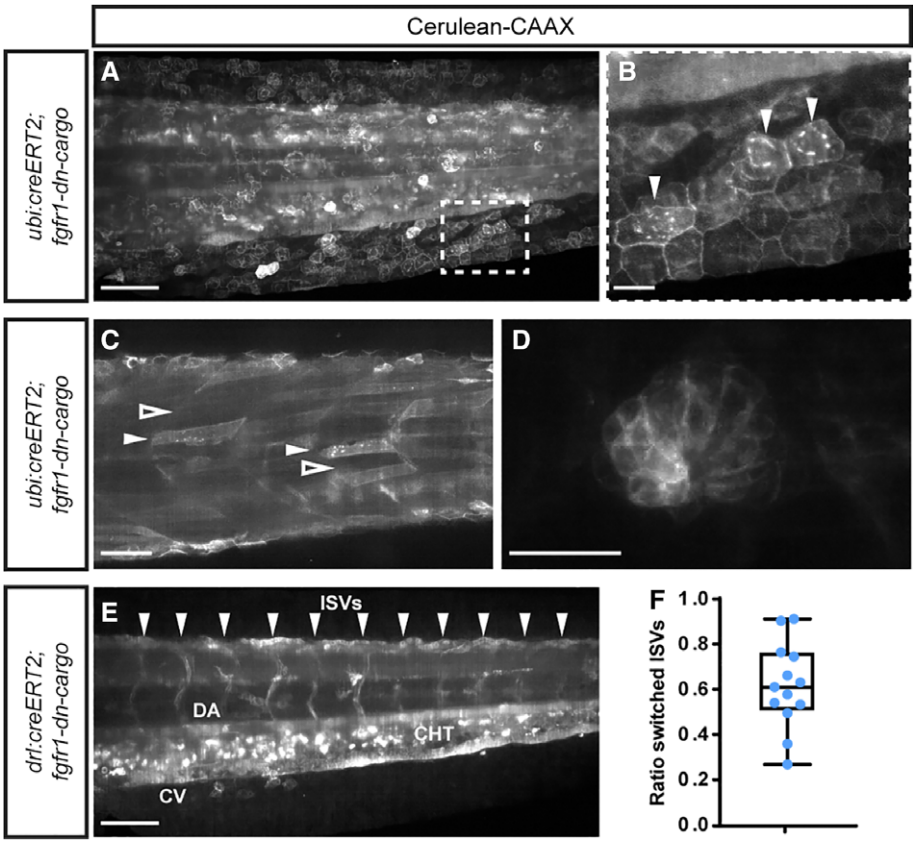

Fig. 2. Recombination efficiency of *fgfr1-dn-cargo.* **A–F**: SPIM imaging of 3-dpf *ubi:creERT2;fgfr-dn-cargo* embryos, 4-OHT induced at shield stage and heatshocked at 3 dpf shortly before imaging; signal shows Cerulean-CAAX fluorescence of the *fgfr1-dn-cargo* transgene upon successful *loxP* recombination. **A,B**: Lateral view of tail, showing the spectrum of Cerulean-CAAX–expressing clones, with hatched outline magnified (B) to document the Cerulean-CAAX signaling confines to membranes and perinuclear ER (arrowheads) of successfully recombined cells. **C,D**: Examples for recombination efficiency in *ubi:creERT2;fgfr-dn-cargo* embryos with Cerulean-CAAX–positive and –negative clones, including somitic muscle fibers (C, white arrowhead for positive fibers, black arrowhead for negative fibers) and a lateral-line neuromast (D). **E,F**: Quantification of recombination efficiency using Cerulean-CAAX lineage labeling in intersomitic vessels (ISVs) in *drl:creERT2;fgfr-dn-cargo* embryos following 4-OHT treatment at shield stage and heatshock at 3 dpf. **E**: Cerulean-CAAX fluorescence was counted in ISVs (arrowheads indicating positions), unilateral or bilateral signal counted as positive labeling. **F**: Ratio of labeled vs. total ISV spaces as proxy for recombination efficiency (n = 13); box depicts standard deviation, bars the maximum spread. Scale bars A,C,E = 100 μm. Scale bars B,D = 20 μm.

signaling activity, as read out by *etv4* expression; nonetheless, we documented reduced FGF signaling 3h and, more prominently, 4 hr after either genetic or chemical FGF signaling perturbation (Fig. 3H,I). Consequently, experiments aiming for FGF signaling perturbations during gastrulation ought to consider slower dynamics and milder effects on FGF signaling attenuation when using the *fgfr1-dn-cargo* transgene.

Perturbation of FGF Signaling in Restricted Cell Lineages

To perform spatiotemporally controlled FGF signaling inhibition using our *fgfr1-dn-cargo* transgene, we next crossed it to the LPM-expressed *drl:creERT2*. To test if *drl:creERT2*-mediated recombination of the *fgfr1-dn-cargo* transgene sufficiently triggers heatshock-dependent Fgfr1a-dn expression in the developing LPM, we performed in toto single-plane illumination microscopy (SPIM) imaging of Cerulean-CAAX as a proxy for transgene expression in *drl:creERT2;fgfr1-dn-cargo* double transgenics. After 4-OHT induction at 30% epiboly and heatshock treatment during somitogenesis (10 ss), we observed LPM-confined mosaic Cerulean expression in the entire LPM at 14 ss (Fig. 4A–C).

Next, we compared phenotypes of SU5402-perturbed wild-type embryos to double-transgenic embryos for *ubi:creERT2; fgfr1-dn-cargo* (ubiquitous FGF perturbation) and *drl:creERT2; fgfr1-dn-cargo* (LPM-specific FGF perturbation), respectively. We primed ubiquitous and lineage-specific *loxP* recombination with 4-OHT at 30% epiboly to shield stage (to target the earliest progenitors expressing *drl:creERT2*), activated *fgfr1-dn-cargo* expression via heatshock at 10–11 ss, and performed phenotype observations at 36 hpf. Defects in embryos following ubiquitous *fgfr1-dn-cargo* transgene activation (n = 78) or a 4-hr pulse of SU5402 at the same stage (n = 403) resembled the phenotypes seen before (Fig. 1I): a mis-looped heart, lack of blood flow, and head and tail defects (Fig. 4D–F,H). In contrast, in embryos perturbed selectively in the *drl* descendants, we observed milder phenotypes mainly characterized by heart defects apparent through blood pooling and edema at the cardiac cavity (n = 24) or no phenotypes (n = 86) (Fig. 4G,H; n = 110, N = 2). Although we also detected defects in the posterior endothelium, we never observed a complete block of blood circulation or posterior tail defects in *drl:creERT2;fgfr1-dn-cargo* double transgenics.

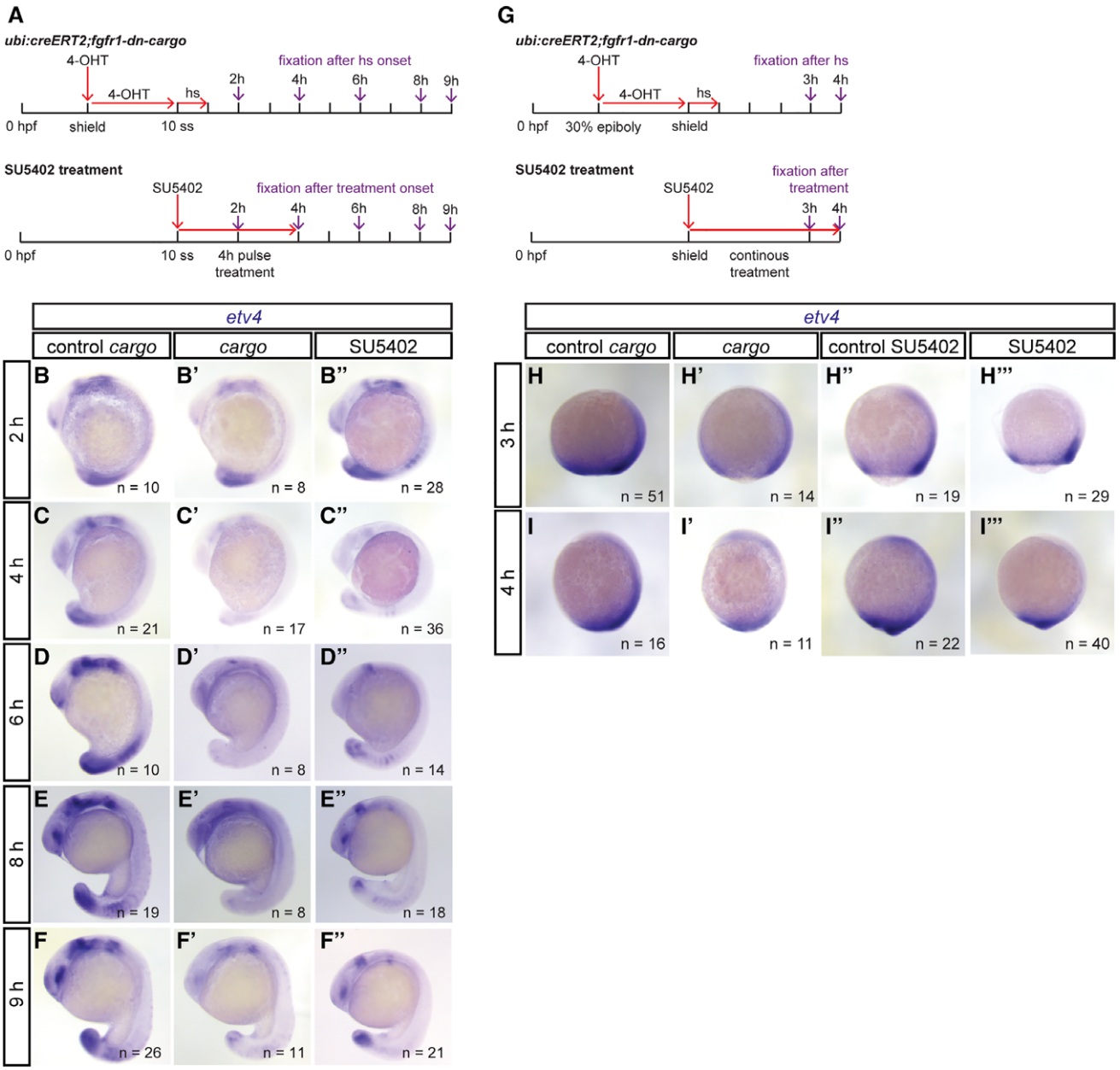

Fig. 3. Temporal dynamics of genetic FGF signaling perturbation using *fgfr1-dn-cargo*. **A**: Schematic showing the time line of treatments for genetic and chemical FGF signaling perturbations and time points of embryo fixation for signaling activity readouts. Red arrows indicate time points and duration of drug (10 μM 4-OHT and 5 μM SU5402) and heatshock treatments; violet arrows mark time points of embryo fixation after treatment onset (heatshock or SU5402 application). **B–F**: Representative embryos stained for *etv4* mRNA expression via in situ hybridization in Cerulean-negative single-transgenic controls (control *cargo*), *ubi:creERT2;fgfr1-dn-cargo* (*cargo*), and SU5402-treated embryos; lateral views, anterior to the top. Number "n" indicates individual embryos stained and analyzed for each condition. B,C: After FGF inhibition was initiated at mid-somitogenesis (10 ss), *etv4* expression in *ubi:creERT2;fgfr1-dn-cargo* and SU5402-treated embryos was decreased 2 hr and absent 4 hr after treatment onset. **D-F**: *etv4* expression started recovering 2 hr after SU5402-treatment was stopped (6 hr after initiation of a 4-hr pulse) and 8 hr after heatshock in *ubi:creERT2;fgfr1-dn-cargo* double transgenics; 9 hr after treatment onset, *etv4* expression recovered to a large extent in genetically and pulse-treated chemically perturbed embryos (F). **G–I**: FGF signaling perturbation during gastrulation stages. G: Schematic showing the time line of treatments (as in A). **H,I**: Representative embryos stained for *etv4* mRNA expression with in situ hybridization in Cerulean-negative single-transgenic controls (control cargo), Cerulean-positive *ubi:creERT2;fgfr1-dn-cargo* double transgenics (*cargo*), untreated wild-type controls (control SU5402), and SU5402-treated embryos; lateral views, anterior to the top. Number "n" indicates individual embryos stained and analyzed for each condition. *etv4* expression in *ubi:creERT2;fgfr1-dn-cargo* and SU5402-treated embryos was decreased 3 hr and 4 hr after treatment at shield stage, but never completely lost as at later stages (see also C,D). Note that Cerulean-CAAX expression could not be observed 1–2 hr post-heatshock, thus *etv4* expression analysis is only shown after 3 hr.

Expression of a dominant-negative receptor could potentially act non-cell-autonomously by scavenging FGF ligand from the extracellular space, rendering it unavailable to neighboring cells. We therefore revisited the expression of *etv4*: In *drl:creERT2;fgfr1-dn-cargo* double transgenics 4-OHT–treated at shield stage and heatshock-treated at 10-11 ss, we did not detect any overt changes to *etv4* expression up to 5 hr after transgene activation (Fig. 4I,J). Observing identically treated embryos at 36 hpf (more

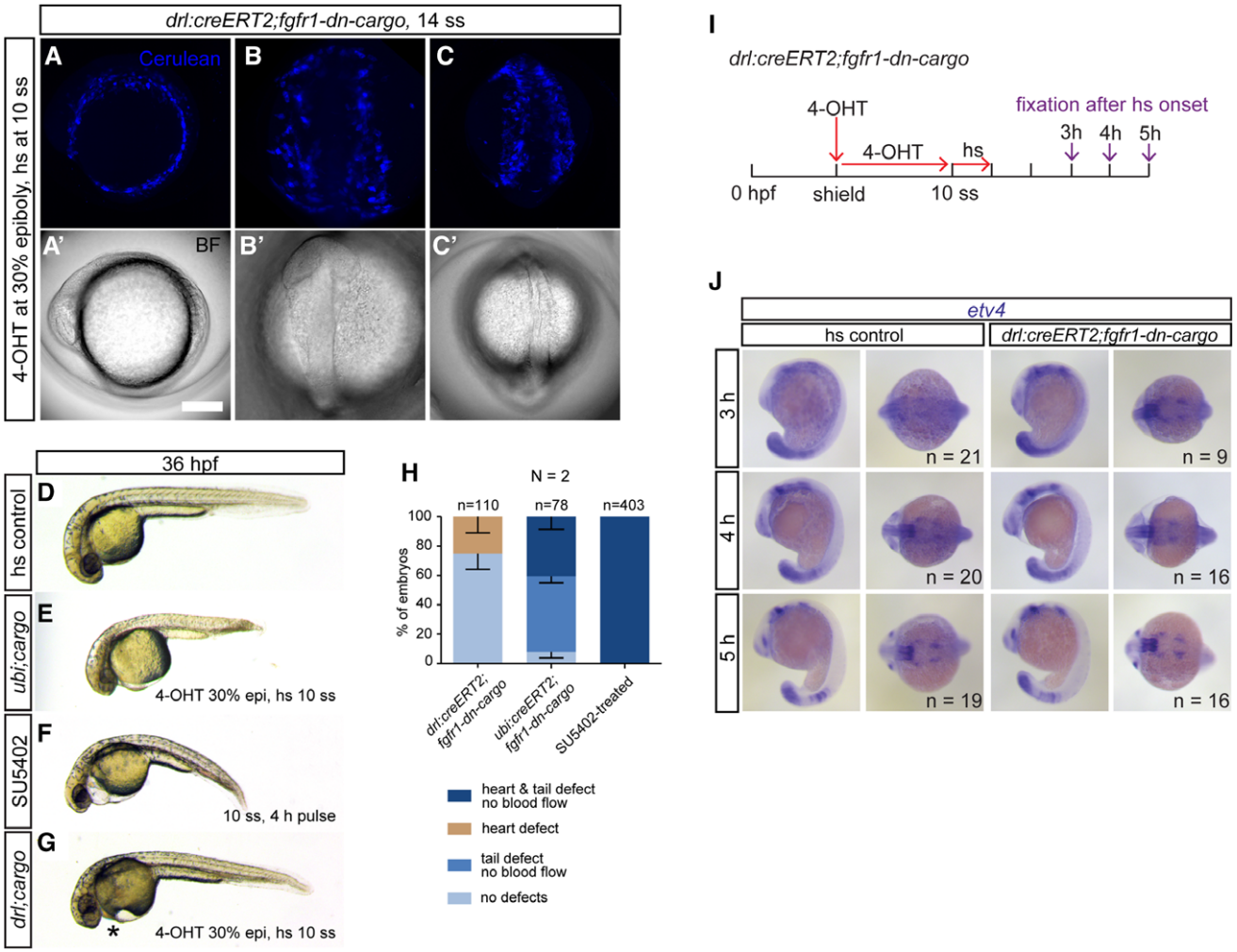

Fig. 4. Tissue-specific FGF signaling perturbation in the developing LPM. **A–C**: Maximum-intensity projection and brightfield images of an in toto SPIM-imaged *drl:creERT2;fgfr1-dn-cargo* double-transgenic embryo. The cell membrane of all Fgfr1a-dn–expressing cells is fluorescently labeled with Cerulean-CAAX after heatshock treatment, revealing mosaic transgene expression throughout the developing LPM; (A) lateral view, anterior to the top; (B) dorsal view of the anterior embryo, anterior to the top; (C) dorsal view of the posterior embryo, anterior to the top. **D–G**: Brightfield images of global or tissue-specific FGF signaling–perturbed embryos, lateral views, anterior to the left. E,F: Ubiquitously Fgfr1-dn–expressing or SU5402-treated embryos show severe cardiovascular defects accompanied by body axis shortening and defects in posterior tail formation. G: Selective cardiovascular phenotypes (asterisk) with no apparent body axis deformations are apparent after tissue-specific FGF signaling perturbation in *drl*–expressing descendants. **H**: Quantifications of phenotypes observed after *drl:creERT2;fgfr1-dn-cargo-*, *ubi:creERT2;fgfr1-dn-cargo-*, or SU5402-mediated FGF signaling inhibition. Number "n" indicates the number of individual embryos analyzed per condition; "N" indicates the number of individual experiments performed. **I–J**: Embryo-wide FGF target gene expression remains grossly intact upon LPM-specific FGF signaling perturbation. I: Schematic showing the time line of treatments for genetic FGF signaling perturbations in *drl:creERT2;fgfr1-dn-cargo* and time points of embryo fixation for signaling activity readouts. Red arrows indicate time points and duration of 4-OHT and heatshock treatments; violet arrows mark time points of embryo fixation after initiation of transgene activation via heatshock. J: Embryos selectively perturbed for FGF signaling in the *drl* descendants at somitogenesis displayed no detectable differences in *etv4* expression when compared to unperturbed siblings 3–5 hr after heatshock treatment (lateral and dorsal views, anterior to the left). Number "n" indicates number of individual embryos analyzed for each condition.

than 21.5 hr post-heatshock), expression of the FGF targets *etv4* and *spry4* remained broadly normal, in contrast to the effect of constant exposure to SU5402 (Figs. 5–6). Nonetheless, we observed reduced expression of *etv4* and *spry4* in the pectoral fin buds of *drl:creERT2;fgfr1-dn-cargo* double-transgenic embryos (Fig. 5A,C,F, Fig. 6A,C,F). We further detected these *etv4* and *spry4* phenotypes upon similarly timed ubiquitous FGF inhibition in *ubi:creERT2;fgfr1-dn-cargo* double transgenics (n = 50/60) and upon pulsed SU5402 treatment (n = 21/56), yet both these conditions also perturbed non-LPM domains of the probed FGF targets (Fig. 5D–F, Fig. 6D–F). Continuous treatment with SU5402 caused complete loss of the pectoral fin domain shown by *etv4* and *spry4* and also the anticipated overall loss of their expression concomitant with perturbed embryo morphology (Fig. 5E,F, Fig. 6E,F).

These data indicate that tissue-specific Fgfr1a-dn expression does not cause pan-embryonic attenuation of FGF signaling activity, arguing against a broad removal of FGF ligand from the extracellular space by the forced tissue-specific expression of dominant-negative Fgfr1a. Our observations further suggest a lasting pectoral-specific effect of FGF perturbation for the window of activity starting at 10–11 ss, possibly influenced by the level of mosaicism following floxed *STOP* cassette excision.

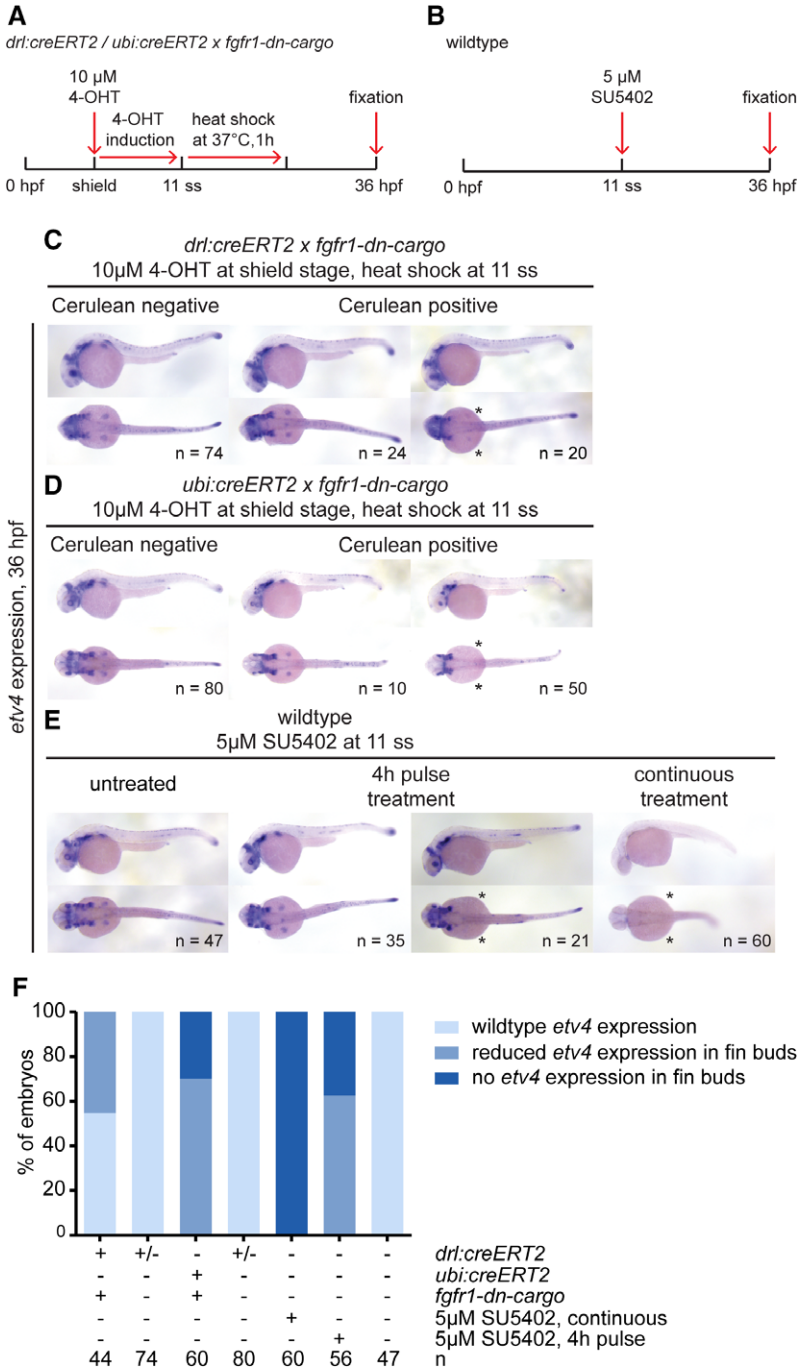

Fig. 5. *etv4* expression in tissue-specific and global FGF signaling–perturbed embryos at 36 hpf. **A,B**: Transgenic embryos were treated with 4-OHT at shield stage and heatshock-treated at 11 ss (A), while wild-type embryos were treated with SU5402 either continuously or for a 4-hr pulse for comparison. B: Expression of the FGF target gene *etv4* assayed at 36 hpf. **C–E**: *etv4* expression in the different conditions. *etv4* expression was grossly unaffected by LPM-specific perturbation using *drl:creERT2* priming *fgfr1-dn-cargo* (C); compare Cerulean-negative to Cerulean-positive, *fgfr1-dn*–expressing embryos, with notable exception of pectoral fin expression that was absent in a cohort of *fgfr1-dn*–expressing embryos (asterisks). *etv4* was also grossly unaffected after ubiquitous FGF perturbation in cohorts of *ubi:creERT2;fgfr1-dn-cargo* embryos (D) and SU5402 pulse-treated embryos (E), while pectoral fin expression was again affected (asterisks in D,E). Continuous FGF signaling inhibition with SU5402 per indicated conditions (B) broadly inhibited *etv4* expression (asterisks in E). **F**: Quantification of *etv4* expression in embryos subjected to embryo-wide or tissue-specific signaling perturbations. Number "n" indicates number of individual embryos analyzed for each condition.

Temporally Distinct Requirements for FGF Signaling Control Pectoral Fin Development in the LPM

While dispensable for initial fin bud induction (Mercader et al., 2006), perturbed FGF signaling starting from approximately 18 ss (18 hpf) and beyond interferes with proper pectoral fin formation, as analyzed in genetic mutants (Fischer et al., 2003; Nomura et al., 2006; Norton et al., 2005) and pan-embryo inhibition using SU5402 (Mercader et al., 2006; Prykhozhij and Neumann, 2008). *fgfr1-dn-cargo* expression in the LPM at 11 ss caused a selective impact on FGF target gene expression in the pectoral fin buds (Fig. 5C,F, Fig. 6C,F). We therefore sought to apply *fgfr1-dn-cargo* to determine if and when LPM lineage–specific perturbation of FGF is sufficient to cause detectable phenotypes in the pectoral fins.

We again crossed hemizygous *drl:creERT2* males with hemizygous *fgfr1-dn-cargo* females, induced in their offspring CreERT2-mediated recombination with 4-OHT at 30% epiboly to maximize LPM priming, performed heatshock treatment to activate *fgfr1-dn-cargo* at discrete time points, and sorted embryos by Cerulean expression as double-transgenic (approximately 25%) vs. *drl:creERT2* or *fgfr1-dn-cargo* siblings; we also performed the same treatment in independent wild-type controls (Fig. 7A). At 48–56 hpf, we observed heart phenotypes based on

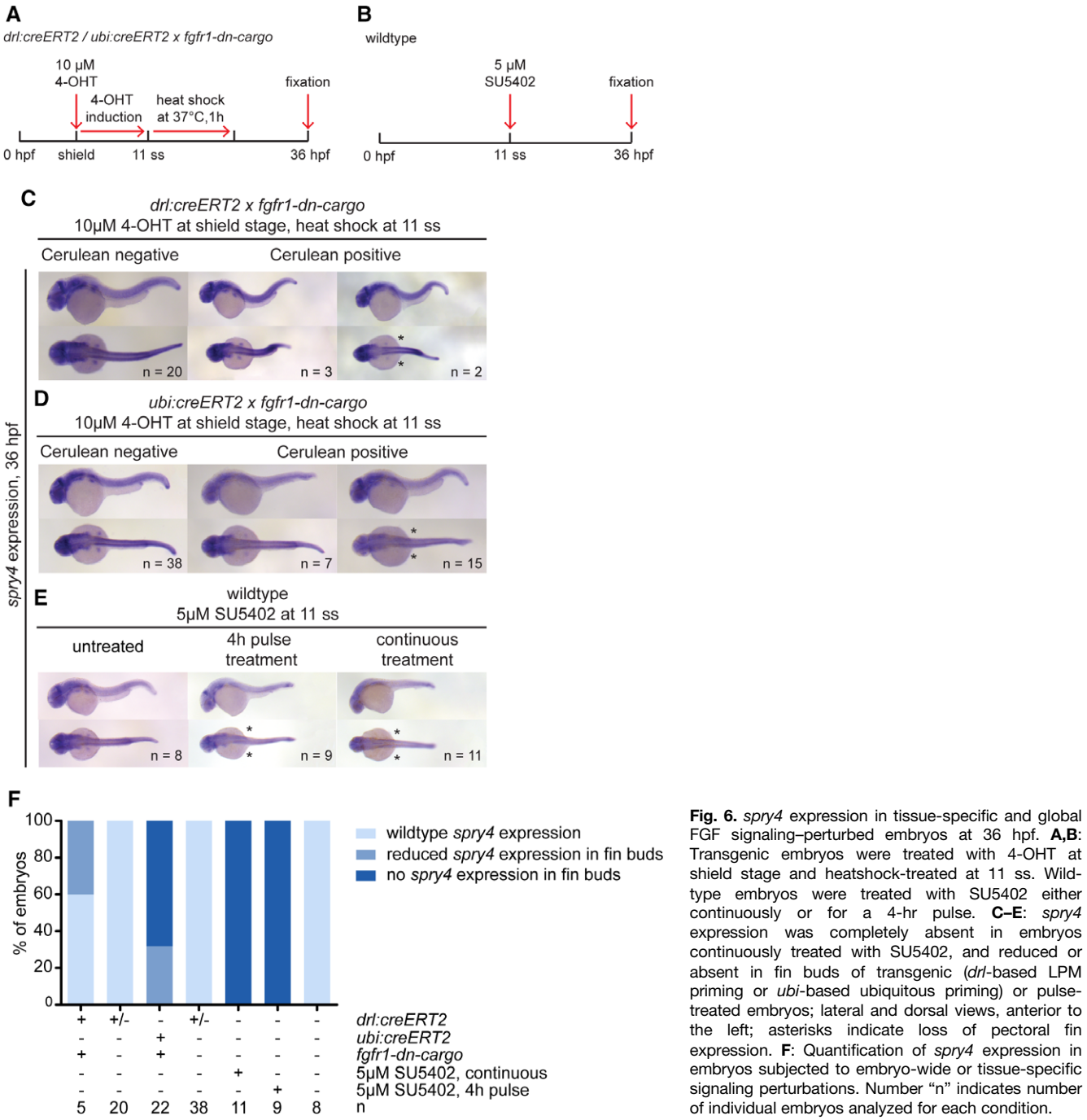

Fig. 6. *spry4* expression in tissue-specific and global FGF signaling–perturbed embryos at 36 hpf. **A,B**: Transgenic embryos were treated with 4-OHT at shield stage and heatshock-treated at 11 ss. Wild-type embryos were treated with SU5402 either continuously or for a 4-hr pulse. **C–E**: *spry4* expression was completely absent in embryos continuously treated with SU5402, and reduced or absent in fin buds of transgenic (*drl*-based LPM priming or *ubi*-based ubiquitous priming) or pulse-treated embryos; lateral and dorsal views, anterior to the left; asterisks indicate loss of pectoral fin expression. **F**: Quantification of *spry4* expression in embryos subjected to embryo-wide or tissue-specific signaling perturbations. Number "n" indicates number of individual embryos analyzed for each condition.

obvious looping defects and development of a cardiac edema as in previous studies (Marques et al., 2008) (Fig. 7B,C); we in detail scored fin defects based on unilateral or bilateral malformation up to complete fin loss (Fig. 7D–G).

With LPM-restricted *fgfr1-dn-cargo* activation at 5 ss, 10 ss, 15 ss, and 20 ss, we consistently observed variable yet reproducible cardiac edema in embryos after heatshock (ranging from 11% to 26%), suggesting functional FGF perturbation consistent with previous observations (Marques et al., 2008). In contrast, we observed no visible pectoral fin defects in embryos with LPM-restricted *fgfr1-dn-cargo* activation at 5 ss, 10 ss, or 15 ss (n = 58, 190, and 172, respectively, from three independent experiments each). Instead, while not fully penetrant, heatshock treatment at 20 ss resulted in unilaterally or bilaterally lost fins (44% of Cerulean-positive embryos; n = 227, three independent experiments; Fig. 7G). This observation upon transient, LPM lineage–focused FGF inhibition starting at 20 ss (approximately 19 hpf) coincides with previously reported mutant and chemical perturbation experiments that assigned the early critical window of FGF signaling during pectoral fin formation between 18 and 28 hpf (Fischer et al., 2003; Norton et al., 2005).

Discussion

The precise spatiotemporal modulation of signaling pathways in vivo, most desirably within selected cell lineages at

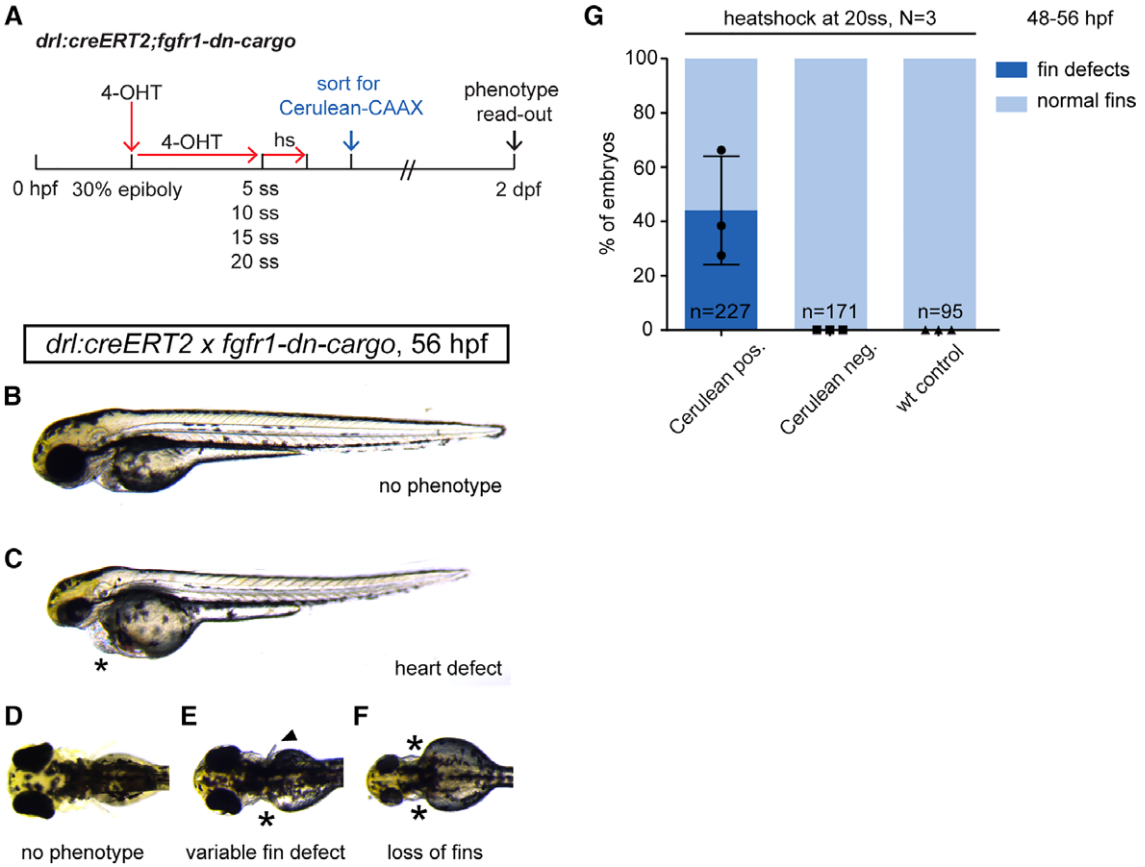

Fig. 7. Temporal dissection of tissue-specific FGF signaling control of cardiac and fin development. **A**: Schematic showing experimental time line of tissue-specific FGF signaling perturbations at discrete developmental stages. 4-OHT induction at 30% epiboly triggers Cre/*lox* recombination in earliest *drl*-expressing progenitors. Heatshock treatments at distinct time points throughout somitogenesis target different phases of cardiac and fin development. **B–D**: Phenotypes scored in 2-dpf *drl:creERT2;fgfr1-dn-cargo* embryos treated as indicated in the schematic above. B,C: Heart defects as scored through blood pooling and cardiac edema on top of the yolk (asterisks); lateral views, anterior to the top. **D–F**: Fin defects were counted upon unilateral; or bilateral fin deformations (arrow head in E, compare to normal pectoral fins in D) and/or loss (asterisks in E,F). **G**: Quantifications of phenotypes in *drl:creERT2;fgfr1-dn-cargo* double transgenics heatshock-treated at different time points during somitogenesis. LPM-specific FGF perturbation triggered by heatshock at 20 ss results in pectoral fin defects in on average 44.09% (s.d. 20.01, p = 005, total n = 227, three independent experiments) of double-transgenic embryos with prior Cerulean expression; earlier heatshock timings caused no discernible fin defects. Number "n" indicates the number of individual embryos analyzed per condition; N indicates the number of individual experiments performed. Statistics based on one-way ANOVA, multiple-comparison Tukey's post-test.

developmental times of interest, remains challenging. Key technical issues are the strict control and kinetics of signaling-modulating transgene expression. To date, existing studies on FGF signaling in zebrafish have predominantly reached their conclusions using elegant mutant genetics and chemical whole-embryo perturbations, such as in the analysis of heart and pectoral fin formation (Dong et al., 2007; Fischer et al., 2003; Marques et al., 2008; Mercader et al., 2006; Norton et al., 2005; de Pater et al., 2009; Reifers et al., 2000). Nonetheless, the cell- or lineage-autonomous contribution of FGF signaling in these processes remains inferred. We have generated *fgfr1-dn-cargo*, a novel zebrafish line carrying a Cre/*lox*-controlled transgene driving dominant-negative Fgfr1a (Lee et al., 2005; Ota et al., 2009) expression to spatiotemporally block FGF signaling. Building on previous direct *hsp70l*-driven and Cre/*lox*-controlled approaches (Hans et al., 2011; Hesselson et al., 2009; Lee et al., 2005), control on two levels defines the cell lineage and time of FGF signaling perturbation: time of 4-OHT induction primes the transgene in the exact lineage per used CreERT2 driver, and time of heatshock treatment determines the developmental stage affected by rapid, pulsed FGF signaling perturbation. The *2A-Cerulean-CAAX* cassette provides a readout for successful transgene expression and assessment of mosaicism by fluorescent membrane labeling (Fig. 1A,B).

Ubiquitous *fgfr1-dn-cargo* transgene activation results in phenotypes and changed expression of FGF target gene resembling global chemical FGFR inhibition with SU5402 in our hands (Fig. 1H–K, Fig. 4E,F) and as previously reported (Brand et al., 1996; Felker et al., 2018; Marques et al., 2008; Reifers et al., 2000). Recombination in our *fgfr1-dn-cargo* line enables fast experimental time lines, permitting transgene activation 1 to 4 h post 4-OHT treatments (Fig. 1C). Moreover, also similar to administration of SU5402, we document successful FGF perturbation within short time frames after heatshock-induced transgene activation (Fig. 1D-G, Fig. 3B,C). These results establish the *fgfr1-dn-cargo* transgenic as viable tool to block FGF signaling genetically in discrete developmental time points and cell types.

While highly potent post-gastrulation, we also documented only partial inhibition of FGF signaling activity during early gastrulation stages using *fgfr1-dn-cargo*, yet also following

SU5402-mediated chemical perturbation (Fig. 3G–I). Due to the maternal contribution of CreERT2 driven by the *ubi* promoter (Mosimann et al., 2011), and since chemical perturbation yielded similar results, we consider low levels of *loxP* recombination an unlikely cause for the incomplete inhibition. Instead, incomplete FGF signaling inhibition may be due to strong FGF signaling activity during gastrulation that is potentially already established through high levels of maternally contributed FGFRs and may not be easily overcome with our transgene. Thus, studies aiming to elucidate spatiotemporal requirements during gastrulation should consider different dynamics from those presented for somitogenesis embryos above.

Expression of our *fgfr1-dn-cargo* transgene is under the control of the *hsp70l* promoter (Fig. 1A), which has been successfully used for driving *loxP*-governed transgenes (Hans et al., 2011; Hesselson et al., 2009). As the activity of the *hsp70l* promoter ceases post-heatshock treatment, *fgfr1-dn* transcription ceases after the heatshock response has faded. This is consistent with the pulsed nature of the perturbation we have observed with our transgene, with complete FGF signaling inhibition up to 6 hr and perturbed signaling up to 9 hr post-heatshock comparable to pulsed SU5402 treatments (Fig. 3D–F). Although *hsp70l* promoter transgenes can respond to other stimuli leading to non-conditional recombination at permissive temperatures (Hans et al., 2009; Hans et al., 2011), we do not observe unspecific Cerulean expression in non-recombined heatshock controls (Fig. 1H) or in recombined non-heatshock-treated transgenics (data not shown), revealing that the used *loxP* STOP cassette (Hesselson et al., 2009) is tight in our particular transgenic insertion. These observations are supported by the lack of phenotypes caused by perturbed FGF signaling in heatshock-only controls (Fig. 4D). Nonetheless, *hsp70l* used to drive *fgfr1-dn-cargo* paired with suitable Cre/CreERT2 drivers provides a versatile combination for fast transgene activation to study fast-occurring, FGF-dependent developmental processes. Moreover, temporally restricted inhibition by *fgfr1-dn-cargo* allows for detailed analysis of exact developmental windows with requirement for FGF signaling activity in a specific cell type.

FGFs expressed in the apical ectodermal ridge (AER) of the developing limb are essential to maintain a progenitor pool that ensures proximal-distal outgrowth and patterning of the mouse and chick limb from the LPM (Crossley et al., 1996; Fallon et al., 1994; Lewandoski et al., 2000; Moon and Capecchi, 2000; Niswander et al., 1993). In particular, ablation of *Fgf8* in the AER leads to severe limb truncations while concurrent removal of *Fgf8, Fgf4*, and *Fgf9* leads to a complete limbless phenotype, demonstrating redundancy and dose dependency (Mariani et al., 2008). Additionally, reciprocal AER FGF signaling activity induces Fgf10 expression in the distal limb mesenchyme which, in return, is necessary to maintain FGF signaling from the AER (Ohuchi et al., 1997; Sekine et al., 1999; Xu et al., 1998). In contrast, FGF signaling functions in earlier steps of limb induction have been controversial. While application of FGF8 to the chicken flank results in ectopic limb formation, and *Fgf8* expression in the intermediate mesoderm had been described to induce limb formation in chick, conditional removal of *Fgf8* activity from the mouse intermediate mesoderm did not abrogate limb development (Crossley et al., 1996; Vogel et al., 1996). Surprisingly, in contrast to FGF8 function in the mouse and chick limb buds, zebrafish *ace* mutants do not feature any pectoral fin defects (Crossley et al., 1996; Lewandoski et al., 2000; Moon and Capecchi, 2000; Reifers et al., 1998). Instead, Fgf24, Fgf10, and Fgf16 have been implicated in zebrafish pectoral fin development, where they act during mesenchyme compaction occurring between 18 and 28 hpf and on AER establishment after 36 hpf (Fischer et al., 2003; Nomura et al., 2006; Norton et al., 2005), but not during early limb induction (Mercader et al., 2006). After priming in the developing LPM, triggering *fgfr1-dn-cargo* expression at 20 ss (19 hpf) resulted in disrupted pectoral fins (Fig. 7D–G), while *fgfr1-dn-cargo* triggered at earlier time points caused no overt pectoral fin defects. Nonetheless, *fgfr1-dn-cargo* is functional in the LPM descendants, as expression of the FGF target genes *etv4* and *spry4* (Figs. 5–6) was reduced at 36 hpf in pectoral fin buds when *fgfr1-dn-cargo* was triggered at 10–11 ss (14–15 hpf); and we observed cardiac phenotypes as reported for SU5402 treatment or genetic perturbations (Marques et al., 2008; de Pater et al., 2009; Pradhan et al., 2017; Reifers et al., 2000) (Fig. 7C). Together, these observations support an LPM-autonomous requirement for FGF activity during the critical phase of pectoral fin bud outgrowth between 18 and 28 hpf in zebrafish, when Fgf10 and Fgf24 are active in the tissue (Fischer et al., 2003; Norton et al., 2005).

A caveat to interpreting Cre/*lox*-based phenotypes remains the variable mosaicism resulting from embryo-to-embryo variation in *loxP* cassette excision, as also observed in our work (Fig. 4A–C). While our phenotypic observation focused on frequently observed overt changes to fin morphology, including complete absence of pectoral fins, we observed an incomplete phenotype penetrance (44% of all *drl:creERT2;fgfr1-dn-cargo*–positive embryos as scored by Cerulean fluorescence, Fig. 7G) in line with mosaicism for *fgfr1-dn-cargo* activity. Besides activity of the used CreERT2 driver, the recombination efficiency of Tol2-based *loxP* transgenes is highly position-dependent (Carney and Mosimann, 2018; Felker and Mosimann, 2016); while our used transgenic insertion is functional, de novo generation of similar or even more potent *cargo* lines requires considerable screening effort. Further, since our experiments applied heatshock treatments relatively soon after CreERT2-mediated priming, future characterization is warranted to define if primed *fgfr1-dn-cargo* remains silent during prolonged phases without heatshock after priming, and how the primed transgene behaves upon repeated heatshock treatments in long-term experiments. All together, the *fgfr1-dn-cargo* line provides a transgenic tool to precisely perturb the FGF pathway during developmental processes based on the paired CreERT2 driver.

Experimental Procedures

Zebrafish Husbandry

Wild-type and transgenic zebrafish were raised and maintained at 28.5 °C without light cycle essentially as described (Westerfield, 2007) and in agreement with procedures mandated by UZH and the veterinary office of the Canton of Zürich. Embryos were kept in E3 medium and strictly staged according to morphological characteristics corresponding to hpf or days postfertilization (dpf) as described previously (Kimmel et al., 1995).

Vectors and Transgenic Lines

Cloning reactions to create transgenesis vectors were performed with the MultiSite Gateway system with LR Clonase II Plus (Life Technologies) according to the manufacturer's instructions. The

fgfr1-dn-cargo plasmid (*pAF019* or *pDestTol2CY_hsp70l:loxP-STOP-loxP-fgfr1a-dn-2A-Cerulean-CAAX, α-crystallin:YFP)* transgene was assembled from *pDH083* (Hesselson et al., 2009) by transfer of the *loxP* cassette into *pENTR5'* (generating *pENTR/5'_hsp70l:loxP-STOP-loxP)*, with *pAF017* (*pME-fgfr1a-dn*), *pAF018* (*p3E-2A-Cerulean-CAAX*), and *pCM326* (Mosimann et al., 2015) as backbone.

25 ng/μL Tol2 mRNA was injected with 25 ng/μL plasmid DNA for Tol2-mediated zebrafish transgenesis (Felker and Mosimann, 2016; Kwan et al., 2007). F0 founders were screened for specific *α-crystallin*:YFP expression, raised to adulthood, and screened for germ line transmission. Single-insertion transgenic strains were established and verified through screening for a 50% germ line transmission rate in outcrosses in subsequent generations per our previously outlined procedures (Felker and Mosimann, 2016). We screened *α-crystallin*:YFP–expressing Tol2-generated F0 founders for functional transgene expression upon *cre* mRNA injection–based *loxP* excision, followed by heatshock-mediated transgene activation to observe Cerulean-CAAX fluorescence and possible phenotypes; more than a dozen founders with independent insertions needed to be screened to recover one functional transgenic line.

Previously established transgenic zebrafish lines used for this study include *ubi:creERT2* (expressing *myl7:EGFP* as transgenic marker) (Mosimann et al., 2011) and *drl:creERT2* (expressing *α-crystallin:Venus* as transgenic marker) (Mosimann et al., 2015).

CreERT2/loxP Experiments

ubi:creERT2 or *drl:creERT2* transgenic zebrafish were individually crossed to the *fgfr1-dn-cargo* line. Embryos were induced using 4-OHT (Sigma H7904) from fresh and/or preheated (65 °C for 10 min) stock solutions in DMSO with a final concentration of 10 μM in E3 embryo medium per our established protocols (Felker et al., 2016; Felker and Mosimann, 2016). Heatshock treatments were performed for 1 h in E3-filled glass tubes in a 37 °C water bath (measured and calibrated with thermometer in the water bath) at specific developmental stages as indicated in individual experiments. Double-transgenic embryos were detected though Cerulean-CAAX expression after heatshock using standard microscopy.

Chemical Treatments

Wild-type embryos were treated with SU5402 to globally perturb FGF signaling at the respective developmental stage. Single-use 100-mM SU5402 stock aliquots were thawed and diluted in E3 to a working concentration indicated in individual experiments directly before administration to the embryos. For pulsed SU5402 treatments, embryos were washed several times in fresh E3 medium after the desired incubation periods. Of note, we observed decreasing potency of stored SU5402 aliquots over time, warranting the use of fresh compound for experiments that require maximal FGF signaling inhibition (data not shown).

Genomic DNA Isolation and Genotyping

Genomic DNA was isolated by incubating single embryos in 50 μL of 50 mM NaOH at 95 °C for 30 min and subsequent neutralization with 5 μl 1M Tris HCl buffer (pH 5.0). Samples were spun down to remove debris and stored at 4 °C until further use.

For genotyping potential *creERT2* transgene carriers, *oAF089* (*5′-GCATTACCGGTCGATGCAACG-3′)* and *oAF090* (*5′-CCAGAGACGGAAATCCATCGC-3′)* primers were used. Primers flanking both *loxP* sites (*oAF040 5′-CGTCGACTCTAGAGGATCACG-3′* and *attB1_rev 5′-AGCCTGCTTTTTTGTACAAACTTG-3′)* were used to genotype for the *fgfr1-dn-cargo* transgene, enabling assessment of successful recombination, as the PCR yields a shorter product (166 bp) after excision of the *loxP*-flanked *STOP* cassette compared to the non-recombined transgene yielding a long product (1129 bp). Standard GoTaq Green Master Mix (Promega) conditions were used for PCR.

In Situ Probe Synthesis

Antisense RNA probes were designed for the genes *etv4/pea3* and *spry4*. First-strand complementary DNA (cDNA) was generated from wild-type zebrafish RNA isolated from different developmental stages using Superscript III First Strand Synthesis kit (Invitrogen) and subsequently pooled (Mosimann et al., 2015). DNA templates were generated using first-strand cDNA as PCR template and the following primers: *etv4* with *oAF169* (*5'-TTACGTATGCAGCCTTCTCG-3')* and *oAF170* (*5'-GGTTCATGGGGTAACTGTGG-3'*); and *spry4* with *oAF183* (*5'-ACTGATGAGGACGAGGAAGG-3')* and *oAF184* (*5'-GACTCGGAATCCTTCAGTGG-3')*. For in vitro transcription initiation, the T7 RNA polymerase promoter *5′-TAATACGACTCACTATAGGG-3'* was added to the 5'-end of reverse primers. PCR reactions were performed under standard conditions using Phusion High-Fidelity DNA Polymerase (Thermo Fisher Scientific). RNA probes were generated via overnight incubation at 37 °C using T7 RNA polymerase (20 U/μl) (Roche) and digoxigenin (DIG)-labeled dNTPs (Roche). The resulting RNA was treated with 1 μM DNAse (Roche) for 15 min at 37 °C and cleaned up in lithium chloride and ethanol to precipitate the RNA.

Embryo Fixation and Whole-mount In Situ Hybridization

Embryos were fixed in 4% paraformaldehyde (PFA) overnight at 4 °C, transferred into 100% methanol, and stored at -20 °C until in situ hybridization. In situ hybridization of whole-mount zebrafish embryos was performed according to published protocols (Thisse and Thisse, 2008).

Microscopy and Image Analysis

Brightfield (BF), basic fluorescence, and in situ hybridization imaging were performed using a Leica M205FA equipped with a DFC450 C camera.

In toto fluorescent embryo imaging was performed by SPIM with a ZEISS Lightsheet Z.1 microscope. Prior to imaging, embryos were embedded in a rod of 1% low-melting agarose in E3 with 0.016% ethyl 3-aminobenzoate methanesulfonate salt (Tricaine; Sigma) in a 50-μL glass capillary. During acquisition, embedded zebrafish were kept at 28 °C in a chamber containing E3 with 0.016% tricaine, or fixed samples were imaged where indicated. Imaging was performed from three to four angles, and images from all illumination sources were fused using the ZEISS Zen Black software. ZEISS Zen Black was also used to construct maximum-intensity projections.

All further image processing was performed with Leica LAS, ImageJ/Fiji, Imaris, and Adobe Photoshop and Illustrator CS6 according to image-preserving guidelines to ensure unbiased editing of the acquired image data.

Statistics

All statistical analysis was performed using GraphPad Prism 6. Data are presented as mean ± SEM, if not noted otherwise. A lower case "n" denotes the number of embryos; a capital "N" signifies the number of replicates. For comparison of two groups, a 2-tailed unpaired Student's *t*-test was performed. A *P* value of 0.05 was considered significant ($P > 0.05$ ns, $P \leq 0.05$*).

Acknowledgements

This work has been supported by a Swiss National Science Foundation (SNSF) professorship (PP00P3_139093) and a Marie Curie Career Integration Grant from the European Commission (CIG PCIG14-GA-2013-631984) to C.M.; a Swiss-European Mobility Program (SEMP) scholarship to M.O.; the Canton of Zürich; the UZH Foundation for Research in Science and the Humanities, and the Swiss Heart Foundation.

We thank Sibylle Burger and Seraina Bötschi for technical and zebrafish husbandry support; Dr. Stephan Neuhauss and the Neuhauss lab for zebrafish support; the Center for Microscopy and Image Analysis (ZMB) at UZH for imaging and equipment support; Dr. Daniela Panáková for assistance with phenotype analysis; and Dr. Duc Dong, Joaquin Navajas Acedo, and all members of the Mosimann lab for critical input.

References

Amaya E, Musci TJ, Kirschner MW. 1991. Expression of a dominant negative mutant of the FGF receptor disrupts mesoderm formation in Xenopus embryos. Cell 66:257–270.

Bökel C, Brand M. 2013. Generation and interpretation of FGF morphogen gradients in vertebrates. Curr Opin Genet Dev 23: 415–422.

Böttcher RT, Niehrs C. 2005. Fibroblast growth factor signaling during early vertebrate development. Endocr Rev 26:63–77.

Brand AH, Perrimon N. 1993. Targeted gene expression as a means of altering cell fates and generating dominant phenotypes. Development 118:401–415.

Brand M, Heisenberg CP, Jiang YJ, Beuchle D, Lun K, Furutani-Seiki M, Granato M, Haffter P, Hammerschmidt M, Kane DA, Kelsh RN, Mullins MC, Odenthal J, van Eeden FJ, Nüsslein-Volhard C. 1996. Mutations in zebrafish genes affecting the formation of the boundary between midbrain and hindbrain. Development 123:179–190.

Branda CS, Dymecki SM. 2004. Talking about a revolution: The impact of site-specific recombinases on genetic analyses in mice. Dev Cell 6:7–28.

Carney TJ, Mosimann C. 2018. Switch and Trace: Recombinase Genetics in Zebrafish. Trends Genet 34:362–378.

Chen J, Xia L, Bruchas MR, Solnica-Krezel L. 2017. Imaging early embryonic calcium activity with GCaMP6s transgenic zebrafish. Dev Biol 430:385–396.

Crossley PH, Minowada G, Macarthur CA, Martin GR. 1996. Roles for FGF8 in the Induction, Initiation, and Maintenance of Chick Limb Development. Cell 84:127–136.

de Pater E, Clijsters L, Marques SR, Lin Y-FF, Garavito-Aguilar Z V, Yelon D, Bakkers J. 2009. Distinct phases of cardiomyocyte differentiation regulate growth of the zebrafish heart. Development 136:1633–1641.

Deng CX, Wynshaw-Boris A, Shen MM, Daugherty C, Ornitz DM, Leder P. 1994. Murine FGFR-1 is required for early postimplantation growth and axial organization. Genes Dev 8:3045–3057.

Dong PDS, Munson CA, Norton W, Crosnier C, Pan X, Gong Z, Neumann CJ, Stainier DY. 2007. Fgf10 regulates hepatopancreatic ductal system patterning and differentiation. Nat Genet 39:397–402.

Fallon JF, López A, Ros MA, Savage MP, Olwin BB, Simandl BK. 1994. FGF-2: apical ectodermal ridge growth signal for chick limb development. Science 264:104–107.

Felker A, Mosimann C. 2016. Contemporary zebrafish transgenesis with Tol2 and application for Cre/lox recombination experiments. Methods Cell Biol. 135:219–244.

Felker A, Nieuwenhuize S, Dolbois A, Blazkova K, Hess C, Low LWLWL, Burger S, Samson N, Carney TJ, Bartunek P, Nevado C, Mosimann C. 2016. In Vivo Performance and Properties of Tamoxifen Metabolites for CreERT2 Control. PLoS One 11: e0152989.

Felker A, Prummel KD, Merks AM, Mickoleit M, Brombacher EC, Huisken J, Panáková D, Mosimann C. 2018. Continuous addition of progenitors forms the cardiac ventricle in zebrafish. Nat Commun 9:2001.

Fischer S, Draper BW, Neumann CJ. 2003. The zebrafish fgf24 mutant identifies an additional level of Fgf signaling involved in vertebrate forelimb initiation. Development 130:3515–3524.

Halpern ME, Rhee J, Goll MG, Akitake CM, Parsons M, Leach SD. 2008. Gal4/UAS Transgenic Tools and Their Application to Zebrafish. Zebrafish 5:97–110.

Hans S, Freudenreich D, Geffarth M, Kaslin J, Machate A, Brand M. 2011. Generation of a non-leaky heat shock-inducible Cre line for conditional Cre/lox strategies in zebrafish. Dev Dyn 240:108–115.

Hans S, Kaslin J, Freudenreich D, Brand M. 2009. Temporally-controlled site-specific recombination in zebrafish. PLoS One 4:e4640.

Henninger J, Santoso B, Hans S, Durand E, Moore J, Mosimann C, Brand M, Traver D, Zon L. 2017. Clonal fate mapping quantifies the number of haematopoietic stem cells that arise during development. Nat Cell Biol 19.

Hess C, Prummel KD, Nieuwenhuize S, Parker H, Rogers KW, Kozmikova I, Racioppi C, Burger S, Brombacher EC, Burger A, Felker A, Chiavacci E, Shah G, Huisken J, Kozmik Z, Christiaen L, Mueller P, Bronner M, Krumlauf R, Mosimann C. 2018. A conserved regulatory program drives emergence of the lateral plate mesoderm. bioRxiv 261115.

Hesselson D, Anderson RM, Beinat M, Stainier DY. 2009. Distinct populations of quiescent and proliferative pancreatic beta-cells identified by HOTcre mediated labeling. Proc Natl Acad Sci U S A 106:14896–14901.

Huang P, Stern MJ. 2005. FGF signaling in flies and worms: More and more relevant to vertebrate biology. Cytokine Growth Factor Rev 16:151–158.

Itoh N, Konishi M. 2007. The zebrafish fgf family. Zebrafish 4: 179–186.

Kawakami K, Asakawa K, Hibi M, Itoh M, Muto A, Wada H. 2016. Gal4 Driver Transgenic Zebrafish. Adv Genet 2016:65–87.

Kimmel CB, Ballard WW, Kimmel SR, Ullmann B, Schilling TF. 1995. Stages of embryonic development of the zebrafish. Dev Dyn 203: 253–310.

Kroll KL, Amaya E. 1996. Transgenic Xenopus embryos from sperm nuclear transplantations reveal FGF signaling requirements during gastrulation. Development 122:3173–3183.

Kwan KM, Fujimoto E, Grabher C, Mangum BD, Hardy ME, Campbell DS, Parant JM, Yost HJ, Kanki JP, Chien C Bin. 2007. The Tol2kit: a multisite gateway-based construction kit for Tol2 transposon transgenesis constructs. Dev Dyn 236:3088–3099.

Ledda F, Paratcha G. 2007. Negative regulation of Receptor Tyrosine Kinase (RTK) signaling: a developing field. Biomark Insights 2:45–58.

Lee Y, Grill S, Sanchez A, Murphy-Ryan M, Poss KD. 2005. Fgf signaling instructs position-dependent growth rate during zebrafish fin regeneration. Development 132:5173–5183.

Lepilina A, Coon AN, Kikuchi K, Holdway JE, Roberts RW, Burns CG, Poss KD. 2006. A Dynamic Epicardial Injury Response Supports Progenitor Cell Activity during Zebrafish Heart Regeneration. Cell 127:607–619.

Lewandoski M, Sun X, Martin GR. 2000. Fgf8 signalling from the AER is essential for normal limb development. Nat Genet 26: 460–463.
Lewis JL, Bonner J, Modrell M, Ragland JW, Moon RT, Dorsky RI, Raible DW. 2004. Reiterated Wnt signaling during zebrafish neural crest development. Development 131:1299–1308.
Mariani FV, Ahn CP, Martin GR. 2008. Genetic evidence that FGFs have an instructive role in limb proximal–distal patterning. Nature 453:401–405.
Marques SR, Lee Y, Poss KD, Yelon D. 2008. Reiterative roles for FGF signaling in the establishment of size and proportion of the zebrafish heart. Dev Biol 321:397–406.
Mercader N, Fischer S, Neumann CJ. 2006. Prdm1 acts downstream of a sequential RA, Wnt and Fgf signaling cascade during zebrafish forelimb induction. Development 133:2805–2815.
Mohammadi M, McMahon G, Sun L, Tang C, Hirth P, Yeh BK, Hubbard SR, Schlessinger J. 1997. Structures of the tyrosine kinase domain of fibroblast growth factor receptor in complex with inhibitors. Science 276:955–960.
Moon AM, Capecchi MR. 2000. Fgf8 is required for outgrowth and patterning of the limbs. Nat Genet 26:455–459.
Mosimann C, Kaufman CK, Li P, Pugach EK, Tamplin OJ, Zon LI. 2011. Ubiquitous transgene expression and Cre-based recombination driven by the ubiquitin promoter in zebrafish. Development 138:169–177.
Mosimann C, Panáková D, Werdich AA, Musso G, Burger A, Lawson KL, Carr LA, Nevis KR, Sabeh MK, Zhou Y, Davidson AJ, DiBiase A, Burns CE, Burns CG, MacRae CA, Zon LI. 2015. Chamber identity programs drive early functional partitioning of the heart. Nat Commun 6:8146.
Mosimann C, Zon LI. 2011. Advanced zebrafish transgenesis with Tol2 and application for Cre/lox recombination experiments. Methods Cell Biol 104:173–194.
Neugebauer JM, Amack JD, Peterson AG, Bisgrove BW, Yost HJ. 2009. FGF signalling during embryo development regulates cilia length in diverse epithelia. Nature 458:651–654.
Niswander L, Tickle C, Vogel A, Booth I, Martin GR. 1993. FGF-4 replaces the apical ectodermal ridge and directs outgrowth and patterning of the limb. Cell 75:579–587.
Nomura R, Kamei E, Hotta Y, Konishi M, Miyake A, Itoh N. 2006. Fgf16 is essential for pectoral fin bud formation in zebrafish. Biochem Biophys Res Commun 347:340–346.
Norton WH, Ledin J, Grandel H, Neumann CJ. 2005. HSPG synthesis by zebrafish Ext2 and Extl3 is required for Fgf10 signalling during limb development. Development 132:4963–4973.
Ohuchi H, Nakagawa T, Yamamoto A, Araga A, Ohata T, Ishimaru Y, Yoshioka H, Kuwana T, Nohno T, Yamasaki M, Itoh N, Noji S. 1997. The mesenchymal factor, FGF10, initiates and maintains the outgrowth of the chick limb bud through interaction with FGF8, an apical ectodermal factor. Development 124:2235–2244.
Oki S, Kitajima K, Meno C. 2010. Dissecting the role of Fgf signaling during gastrulation and left-right axis formation in mouse embryos using chemical inhibitors. Dev Dyn 239:1768–1778.
Ornitz DM, Itoh N. 2001. Protein family review: Fibroblast growth factors. Genome Biol 2:reviews3005.
Ornitz DM, Itoh N. 2015. The Fibroblast Growth Factor signaling pathway. Wiley Interdiscip Rev Dev Biol 4:215–266.
Ota S, Tonou-Fujimori N, Tonou-Fujimori N, Nakayama Y, Ito Y, Kawamura A, Yamasu K. 2010. FGF receptor gene expression and its regulation by FGF signaling during early zebrafish development. Genesis 48:707–716.
Ota S, Tonou-Fujimori N, Yamasu K. 2009. The roles of the FGF signal in zebrafish embryos analyzed using constitutive activation and dominant-negative suppression of different FGF receptors. Mech Dev 126:1–17.
Plotnikov AN, Hubbard SR, Schlessinger J, Mohammadi M. 2000. Crystal structures of two FGF-FGFR complexes reveal the determinants of ligand-receptor specificity. Cell 101:413–424.
Pradhan A, Zeng XI, Sidhwani P, Marques SR, George V, Targoff KL, Chi NC, Yelon D. 2017. FGF signaling enforces cardiac chamber identity in the developing ventricle. Development 144:1328–1338.
Prykhozhij SV, Neumann CJ. 2008. Distinct roles of Shh and Fgf signaling in regulating cell proliferation during zebrafish pectoral fin development. BMC Dev Biol 8:91.
Raible F, Brand M. 2001. Tight transcriptional control of the ETS domain factors Erm and Pea3 by Fgf signaling during early zebrafish development. Mech Dev 107:105–117.
Reifers F, Böhli H, Walsh EC, Crossley PH, Stainier DYR, Brand M. 1998. Fgf8 is mutated in zebrafish acerebellar (ace) mutants and is required for maintenance of midbrain-hindbrain boundary development and somitogenesis. Development 125: 2381–2395.
Reifers F, Walsh EC, Léger S, Stainier DY, Brand M, Leger S, Stainier DYR, Brand M. 2000. Induction and differentiation of the zebrafish heart requires fibroblast growth factor 8 (fgf8/acerebellar). Development 127:225–235.
Richardson R, Metzger M, Knyphausen P, Ramezani T, Slanchev K, Kraus C, Schmelzer E, Hammerschmidt M. 2016. Re-epithelialization of cutaneous wounds in adult zebrafish combines mechanisms of wound closure in embryonic and adult mammals. Development 143:2077–2088.
Roehl H, Nüsslein-Volhard C. 2001. Zebrafish pea3 and erm are general targets of FGF8 signaling. Curr Biol 11:503–507.
Rossant J, Nagy A. 1995. Genome engineering: the new mouse genetics. Nat Med 1:592–594.
Sekine K, Ohuchi H, Fujiwara M, Yamasaki M, Yoshizawa T, Sato T, Yagishita N, Matsui D, Koga Y, Itoh N, Kato S. 1999. Fgf10 is essential for limb and lung formation. Nat Genet 21: 138–141.
Shin D, Shin CH, Tucker J, Ober EA, Rentzsch F, Poss KD, Hammerschmidt M, Mullins MC, Stainier DYR. 2007. Bmp and Fgf signaling are essential for liver specification in zebrafish. Development 134:2041–2050.
Simoes FC, Peterkin T, Patient R, Simões FC, Peterkin T, Patient R. 2011. Fgf differentially controls cross-antagonism between cardiac and haemangioblast regulators. Development 138: 3235–3245.
Sun X, Meyers EN, Lewandoski M, Martin GR. 1999. Targeted disruption of Fgf8 causes failure of cell migration in the gastrulating mouse embryo. Genes Dev 13:1834–1846.
Thisse C, Thisse B. 2008. High-resolution in situ hybridization to whole-mount zebrafish embryos. Nat Protoc 3:59–69.
Ueno S, Weidinger G, Osugi T, Kohn AD, Golob JL, Pabon L, Reinecke H, Moon RT, Murry CE. 2007. Biphasic role for Wnt/-beta-catenin signaling in cardiac specification in zebrafish and embryonic stem cells. Proc Natl Acad Sci 104:9685–9690.
Ullrich A, Schlessinger J. 1990. Signal transduction by receptors with tyrosine kinase activity. Cell 61:203–212.
Vogel A, Rodriguez C, Izpisúa-Belmonte JC. 1996. Involvement of FGF-8 in initiation, outgrowth and patterning of the vertebrate limb. Development 122:1737–1750.
Westerfield M. 2007. The Zebrafish Book: a guide for the laboratory use of zebrafish (Danio rerio). 5th ed. Eugene, OR: University of Oregon Press.
Xu X, Weinstein M, Li C, Naski M, Cohen RI, Ornitz DM, Leder P, Deng C. 1998. Fibroblast growth factor receptor 2 (FGFR2)-mediated reciprocal regulation loop between FGF8 and FGF10 is essential for limb induction. Development 125:753–765.
Zuniga E, Rippen M, Alexander C, Schilling TF, Crump JG. 2011. Gremlin 2 regulates distinct roles of BMP and Endothelin 1 signaling in dorsoventral patterning of the facial skeleton. Development 138:5147–5156.